Inorg. Chem. **2005**, *44*, 1061–1067

Cations $M_2(O_2C^tBu)_4^+$, Where M = Mo and W, and $MoW(O_2C^tBu)_4^+$. Theoretical, Spectroscopic, and Structural Investigations

Malcolm H. Chisholm,* Jason S. D'Acchioli, Brian D. Pate, and Nathan J. Patmore

Department of Chemistry, The Ohio State University, 100 W. 18th Avenue, Columbus, Ohio 43210-1185

Naresh S. Dalal* and David J. Zipse

Department of Chemistry and Biochemistry, National High Magnetic Field Laboratory, Florida State University, Tallahassee, Florida 32306

Received July 12, 2004

With the aid of density function theory, the molecular and electronic structures of the molecules $Mo_2(O_2CMe)_4$, $MoW(O_2CMe)_4$, and $W_2(O_2CMe)_4$ and their single-electron oxidized radical cations have been determined; this includes calculated observables such as ν(MM) and the $\delta \rightarrow \delta^*$ electronic transition energies. The calculated properties are compared with those for the corresponding pivalates, $M_2(O_2C^tBu)_4$ (M = Mo or W) and $MoW(O_2C^tBu)_4$ and their radical cations prepared in situ by oxidation with Cp_2FePF_6. The EPR spectra of the radical cations are also reported. The EPR spectrum of the $MoW(O_2C^tBu)_4^+$ cation reveals that the unpaired electron is in a polarized MM δ orbital having 70% Mo and 30% W character. The MM stretching frequencies show good correlation with the MM bond lengths obtained from single-crystal X-ray diffraction studies of $MoW(O_2C^tBu)_4$, $W_2(O_2C^tBu)_4$, and $W_2(O_2C^tBu)_4{}^+PF_6^-$ compounds, along with previously reported structures. These data provide benchmark parameters for valence trapped dicarboxylate bridged radical cations of the type $[(^tBuCO_2)_3M_2]_2(\mu\text{-}O_2C\text{–}X\text{–}CO_2)^+$ (X = conjugated spacer).

Introduction

Recent work in this laboratory has been aimed at studying the properties of compounds containing linked MM quadruple bonds of the type $[(^tBuCO_2)_3M_2]_2(\mu\text{-}O_2C{-}X{-}CO_2)$, where M = Mo or W and the X group is a spacer that allows for electronic communication between the two M_2 centers.[1] Upon oxidation to the radical cations $[(^tBuCO_2)_3M_2]_2(\mu\text{-}O_2C{-}X{-}CO_2)^+$, the positive charge may be delocalized over all four metal centers, as was recently reported for M = Mo and W and X = nothing (i.e., μ-oxalate) and for M = W and X = C_6F_4 or 2,5-thienyl.[2] For M = Mo and X = C_6F_4 or 2,5-thienyl the charge was localized on each dimetal unit, as deduced by EPR spectroscopy. Related systems having dicarboxylate linked Mo_2 quadruple bonds supported by formamidinate ligands have been examined by Cotton and co-workers.[3] As Cotton elegantly showed for a series of $O_2C{-}(CH{=}CH)_n{-}CO_2$ bridged compounds where $n = 1{-}4$, the degree of coupling of the Mo_2 centers drops off with increasing n, which lengthens the distance between the two dinuclear metal centers.[4] This is, of course, a well-known phenomenon for two linked mixed valence metal centers separated by bridges of varying length.[5]

For any mixed valence system of the type $[L_nM{-}bridge{-}ML_n]^+$, the degree of delocalization of charge can be questioned with respect to time scale. On the Robin and Day classification scheme,[6] the distinction between Class II and Class III, or strongly coupled and completely delocalized,

* Authors to whom correspondence should be addressed. E-mail: chisholm@chemistry.ohio-state.edu (M.H.C.); dalal@chem.fsu.edu (N.D.).

(1) Chisholm, M. H. *J. Chem. Soc., Dalton Trans.* **2003**, 3821.
(2) (a) Chisholm, M. H.; Pate, B. D.; Wilson, P. J.; Zaleski, J. M. *Chem. Commun.* **2002**, 1084. (b) Byrnes, M. J.; Chisholm, M. H. *Chem. Commun.* **2002**, 2040.
(3) (a) Cotton, F. A.; Lin, C.; Murillo, C. A. *Acc. Chem. Res.* **2001**, *34*, 759. (b) Cotton, F. A.; Lin, C.; Murillo, C. A. *Proc. Natl. Acad. Sci. USA* **2002**, *99*, 4810.
(4) Cotton, F. A.; Donahue, J. P.; Murillo, C. A. *J. Am. Chem. Soc.* **2003**, *125*, 5436.
(5) (a) Crutchley, R. J. *Adv. Inorg. Chem.* **1994**, *41*, 273. (b) Hush, N. S. *Coord. Chem. Rev.* **1985**, *64*, 135. (c) Richardson, D. E.; Taube, H. *Coord. Chem. Rev.* **1984**, *60*, 107.
(6) Robin, M. B.; Day, P. *Adv. Inorg. Radiochem.* **1967**, *10*, 247.

10.1021/ic049081g CCC: $30.25
Published on Web 01/22/2005

is clearly dependent upon the reference of time scale. The distinction between very strongly coupled or almost delocalized and fully delocalized continues to be a matter of considerable interest.[7] Single-crystal X-ray crystallography can readily distinguish between the two M_2 units in a Class I, $[L_nM_2(\mu\text{-bridge})M_2L_n]^+$ species where the MM bonding configurations are $\sigma^2\pi^4\delta^2$ and $\sigma^2\pi^4\delta^1$, providing there is no positional disorder in the molecular structure.[8] However, given the very small differences expected in M−M and M−L bond distances (∼0.05 and 0.01 Å, respectively), a disordered structure is rather likely to be commonly encountered. The metals Mo and W both have spin active nuclei [^{95}Mo, ^{97}Mo, $I = {}^5/_2$ ($\Sigma_{abund} \sim 25\%$) and ^{183}W, $I = {}^1/_2$, 14.5% abundance], which makes EPR spectroscopy a very powerful tool for ascertaining electron delocalization in an oxidized compound having a single electron shared between either two or four metal atoms. However, the time scale of EPR spectroscopy is on the order of 10^{-10} s, which is still slow with respect to the vibronic or electronic time scale of $\sim 10^{-15}$ s. It is, therefore, desirable to have spectroscopic data for the relevant $M_2(O_2C^tBu)_4^+$ cations (M = Mo, W). Rather interestingly, little information exists for such species and only very recently in a paper entitled "Filling a Void" did Cotton and co-workers report the crystal and molecular structure of a $Mo_2(O_2CR)_4$ compound and its stable cationic complex $Mo_2(O_2CR)_4^+BF_4^-$, where R = 2,4,6-triisopropylbenzene (C_6H_2-2,4,6-^{i}Pr$_3$).[9] We report here our spectroscopic and crystallographic studies of $M_2(O_2C^tBu)_4$ and $M_2(O_2C^t\text{-}Bu)_4^+PF_6^-$ (M = Mo, W) compounds, along with the mixed metal $MoW(O_2C^tBu)_4^{0/+}$ complexes and the calculated data for the related model acetate compounds. Aside from the intrinsic interest in the spectroscopic properties of the $M_2(O_2CR)_4^{0/+}$ compounds, the data presented herein are particularly relevant in providing points of reference with respect to the degree of hole delocalization in $[(^tBuCO_2)_3M_2(\mu\text{-bridge})M_2(O_2C^tBu)_3]^+$ cations.

Experimental Section

Physical Procedures. The cyclic voltammogram and differential pulse voltammogram of $MoW(O_2C^tBu)_4$ were collected with a scan rate of 100 mV s^{-1} and 5 mV s^{-1}, respectively, using a Princeton Applied Research (PAR) 173A potentiostat-galvanostat equipped with a PAR 176 current-to-voltage converter. Electrochemical measurements were performed under an inert atmosphere in a 0.1 M solution of $^nBu_4NPF_6$ in THF inside a single-compartment voltammetric cell, equipped with a platinum working electrode, a platinum wire auxiliary electrode, and a pseudo-reference electrode consisting of a silver wire in a 0.1 M $^nBu_4NPF_6$/THF solution. The potential values are referenced to the $FeCp_2/FeCp_2^+$ couple, obtained by addition of a small amount of $FeCp_2$ to the solution.

Raman spectra were collected with a Renishaw 1000B micro-Raman spectrometer operating with a 785-nm SDL diode laser under variable power (0.2−20 mW) conditions.

$Mo_2(O_2C^tBu)_4$,[10] $MoW(O_2C^tBu)_4$,[11] and $W_2(O_2C^tBu)_4$[12] were prepared using previously published literature procedures. The radical cations were generated in situ by addition of 1 equiv of $FeCp_2PF_6$ before measurements because of their instability.

EPR Studies. EPR measurements were carried out at X-band (9.5 GHz). The spectra were obtained on solution and frozen glass samples using a Bruker Elexsys-500 EPR spectrometer. For precise determination of the g-values and splittings, the magnetic field was calibrated with a built-in Bruker NMR gaussmeter, and the frequency was measured with a digital frequency counter. The temperature of the solution and frozen glass spectra was varied from 4 K to room temperature using an Oxford continuous flow He cryostat to an accuracy of ±0.1 K.

Molecular and Electronic Structure Calculations. Molecular and electronic structure determinations on the model complexes $M_2(O_2CMe)_4$ (M = Mo or W) and $MoW(O_2CMe)_4$, as well as their respective radical cations, were performed using density functional theory (DFT) as implemented in the Gaussian 2003 suite of programs.[13] We have used the B3LYP[14] functional along with the 6-31G* basis set for H, C, and O,[15] and the SDD energy-consistent pseudopotentials for Mo and W.[16] All geometries were fully optimized in C_{4v} symmetry (for the sake of simplifying orbital and vibrational symmetry analyses) at the above levels using the default optimization criterion. Vibrational frequency analyses indicated the C_{4v} structures were not local minima on their respective potential energy surfaces; low-energy imaginary vibrations attributed to "methyl twitchings" were observed at ca. 37 cm^{-1}. Geometry optimizations at lower symmetry were, in most cases, not performed due to convergence criteria issues which were attributed to distortions in methyl-group orientations. However, calculations in C_1 symmetry which did converge showed a less than 1 kcal mol^{-1} energy difference compared to the C_{4v} structures, lending credibility to the use of C_{4v} symmetry. Orbital and vibrational frequency analyses were completed with GaussView.[17] Electronic absorption spectra were predicted using the TD-DFT method as implemented within Gaussian 2003 using the default optimization criteria.[18] Mulliken population analyses[19] were facilitated through the use of

(7) (a) Nelson, S. F. *Chem. Eur. J.* **2001**, *6*, 581. (b) Brunschwig, B. S.; Creutz, C.; Sutin, N. *Chem. Soc. Rev.* **2002**, *31*, 168.

(8) (a) Cotton, F. A.; Dalal, N. S.; Liu, C. Y.; Murillo, C. A.; North, J. M.; Wang, X. *J. Am. Chem. Soc.* **2003**, *125*, 12945. (b) Cotton, F. A.; Walton, R. A. *Multiple Bonds Between Metal Atoms*, 2nd ed.; Oxford University Press: Oxford, 1993.

(9) Cotton, F. A.; Daniels, L. M.; Hillard, E. A.; Murillo, C. A. *Inorg. Chem.* **2002**, *41*, 1639.

(10) Brignole, A. G.; Cotton, F. A. *Inorg. Synth.* **1972**, *13*, 81.

(11) Katovic, V.; Templeton, J. L.; Hoxmeler, R. J.; McCarley, R. E. *J. Am. Chem. Soc.* **1975**, *97*, 5300.

(12) Santure, D. J.; Huffman, J. C.; Sattelberger, A. P. *Inorg. Chem.* **1985**, *24*, 371.

(13) Frisch, M. J.; Trucks, G. W.; Schlegel, H. B.; Scuseria, G. E.; Robb, M. A.; Cheeseman, J. R.; Montgomery, J. A., Jr.; Vreven, T.; Kudin, K. N.; Burant, J. C.; Millam, J. M.; Iyengar, S. S.; Tomasi, J.; Barone, V.; Mennucci, B.; Cossi, M.; Scalmani, G.; Rega, N.; Petersson, G. A.; Nakatsuji, H.; Hada, M.; Ehara, M.; Toyota, K.; Fukuda, R.; Hasegawa, J.; Ishida, M.; Nakajima, T.; Honda, Y.; Kitao, O.; Nakai, H.; Klene, M.; Li, X.; Knox, J. E.; Hratchian, H. P.; Cross, J. B.; Adamo, C.; Jaramillo, J.; Gomperts, R.; Stratmann, R. E.; Yazyev, O.; Austin, A. J.; Cammi, R.; Pomelli, C.; Ochterski, J. W.; Ayala, P. Y.; Morokuma, K.; Voth, G. A.; Salvador, P.; Dannenberg, J. J.; Zakrzewski, V. G.; Dapprich, S.; Daniels, A. D.; Strain, M. C.; Farkas, O.; Malick, D. K.; Rabuck, A. D.; Raghavachari, K.; Foresman, J. B.; Ortiz, J. V.; Cui, Q.; Baboul, A. G.; Clifford, S.; Cioslowski, J.; Stefanov, B. B.; Liu, G.; Liashenko, A.; Piskorz, P.; Komaromi, I.; Martin, R. L.; Fox, D. J.; Keith, T.; Al-Laham, M. A.; Peng, C. Y.; Nanayakkara, A.; Challacombe, M.; Gill, P. M. W.; Johnson, B.; Chen, W.; Wong, M. W.; Gonzalez, C.; Pople, J. A. *Gaussian 2003*, Revision B.04 ed.; Gaussian, Inc.: Pittsburgh, PA, 2003.

(14) (a) Becke, A. D. *Phys. Rev. A* **1988**, *38*, 3098. (b) Becke, A. D. *J. Chem. Phys.* **1993**, *98*, 5648. (c) Lee, C.; Yang, W.; Parr, R. G. *Phys. Rev. B: Condens. Matter* **1988**, *37*, 785.

(15) Hehre, W. J.; Radom, L.; Schleyer, P. v. R.; Pople, J. A. *Ab initio Molecular Orbital Theory*; John Wiley & Sons: New York, 1986.

(16) Andrae, D.; Hauessermann, U.; Dolg, M.; Preuss, H. *Theor. Chim. Acta* **1990**, *77*, 123.

(17) *Gaussview 3.0*; Gaussian, Inc.: Pittsburgh, PA, 2003.

Table 1. Crystallographic Details for $MoW(O_2C^tBu)_4$, $W_2(O_2CBu^t)_4$, and $W_2(O_2CBu^t)_4^+PF_6^-$

	$MoW(O_2CBu^t)_4$	$W_2(O_2C^tBu)_4$	$W_2(O_2C^tBu)_4^+PF_6^-$
empirical formula	$C_{20}\,H_{36}\,O_8\,Mo_1\,W_1$	$C_{20}\,H_{36}\,O_8\,W_2$	$C_{20}\,H_{36}\,F_6\,O_8\,P_1\,W_2$
formula weight	684.27	772.19	917.16
temperature (K)	200	200	200
wavelength (Å)	0.71073	0.71073	0.71073
crystal system	triclinic	triclinic	monoclinic
space group	$P\bar{1}$	$P\bar{1}$	$C2/c$
unit cell dimensions			
a (Å)	5.729(1)	5.731(1)	16.767(2)
b (Å)	10.846(2)	10.817(2)	10.379(2)
c (Å)	11.196(2)	11.206(3)	19.117(3)
α (deg)	70.49(1)	70.61(1)	90
β (deg)	86.85(1)	86.52(1)	115.61(1)
γ (deg)	89.01(1)	89.05(1)	90
volume (Å^3)	654.8(2)	654.1(2)	3000.0(8)
Z	1	1	4
D_{calc} (Mg m^{-3})	1.735	1.960	2.031
absorption coefficient (mm^{-1})	4.904	8.823	7.791
F(000)	336	368	1748
crystal size (mm^3)	0.06 × 0.08 × 0.15	0.04 × 0.08 × 0.15	0.08 × 0.12 × 0.19
θ range for data collection (deg)	3.21 to 27.38	2.27 to 25.00	2.36 to 27.48
index ranges	$-7 \le h \le 7$, $-14 \le k \le 14$, $-14 \le l \le 14$	$-6 \le h \le 6$, $-12 \le k \le 12$, $-13 \le l \le 13$	$-21 \le h \le 21$, $-13 \le k \le 13$, $-24 \le l \le 24$
reflections collected	5824	4442	6448
independent reflections	2965 [$R_{int} = 0.0182$]	2303 [$R_{int} = 0.0201$]	3444 [$R_{int} = 0.0198$]
refinement method	full-matrix least-squares on F^2	full-matrix least-squares on F^2	full-matrix least-squares on F^2
data/restraints/parameters	2965/0/137	2303/1/148	3444/0/169
goodness-of-fit on F^2	1.056	1.066	1.066
final r indices [$I > 2\sigma(I)$]	R1 = 0.0236, wR2 = 0.0593	R1 = 0.0216, wR2 = 0.0433	R1 = 0.0249, wR2 = 0.0534
R indices (all data)	R1 = 0.0275, wR2 = 0.0608	R1 = 0.0266, wR2 = 0.0447	R1 = 0.0367, wR2 = 0.0564
largest diff. peak and hole (e Å^{-3})	1.295 and −1.009	1.770 and −1.090	1.634 and −0.728

the orbpopg03[20] program made available through Professor Jeffrey Hay at the University of California.

X-ray Crystallography. All work was done using a Nonius Kappa CCD diffractometer at 200 K using an Oxford Cryostreams Cryostream cooler. A combination of φ and ω scans with a frame width of 1.0° was used. Data integration was done with Denzo,[21] and scaling and merging of the data were done with Scalepack[21] in all instances. Each structure was solved using direct methods in Shelxs-97[22] and full-matrix least-squares refinements based on F^2 were performed in Shelxl-97[22] in the WinGX suite of programs.[23] All methyl hydrogens were included in the models at calculated positions using a riding model with $U(H) = 1.5 \times U_{eq}$ (bonded carbon atom).

The data collection crystal for $MoW(O_2C^tBu)_4$ was a yellow rectangular plate. The diffraction pattern indicated a triclinic crystal system, and the data collection was set up to measure a hemisphere of reciprocal space with a redundancy factor of 3.2, which means that 90% of the reflections were measured at least 3.2 times. The structure was solved in the $P\bar{1}$ space group. The molecule contains a crystallographically imposed center of inversion and hence each molybdenum and tungsten atom is disordered over the same atomic site, modeled as a composite 0.5 Mo/0.5 W atom, and refined anisotropically along with all other non-hydrogen atoms.

The data collection crystal for $W_2(O_2C^tBu)_4$ was a yellow rod. The diffraction pattern indicated a triclinic crystal system, and the data collection was set up to measure a hemisphere of reciprocal space with a redundancy factor of 2.9. The structure was solved in the $P\bar{1}$ space group. The molecule contains a crystallographically imposed center of inversion, and one of the ^{t}Bu groups was disordered over two positions. All non-hydrogen atoms were refined anisotropically.

The data collection crystal for $W_2(O_2C^tBu)_4^+PF_6^-$ was a green block. The diffraction pattern indicated a monoclinic crystal system, and the data collection was set up to measure a quadrant of reciprocal space with a redundancy factor of 4.9. The structure was solved in the $C2/c$ space group. The molecule contains a crystallographically imposed center of inversion, and all non-hydrogen atoms were refined anisotropically.

Experimental data relating to the structure determinations are displayed in Table 1.

Results and Discussion

Calculated Data for $M_2(O_2CMe)_4$ (Mo = Mo, W), $MoW(O_2CMe)_4$, and Their Cations. Density functional theory calculations using the Gaussian 2003 suite of programs[13] have been used to elucidate the molecular structures of the model compounds $M_2(O_2CMe)_4$ (M = Mo and W), $MoW(O_2CMe)_4$, and their radical cations; all structures were restricted to C_{4v} symmetry (Figure 1). The calculated metal−metal and metal−oxygen distances are listed in Table 2, together with the calculated values for ν(MM) and the wavelength of the $\delta \rightarrow \delta^*$ electronic transitions.

The calculations predict that, upon oxidation, there is an increase in MM distance of roughly 0.05 Å, which is consistent with the removal of an electron from a δ-bonding

(18) (a) Bauernschmitt, R.; Ahlrichs, R. *Chem. Phys. Lett.* **1996**, *256*, 454. (b) Casida, M. E.; Jamorski, C.; Casida, K. C.; Salahub, D. R. *J. Chem. Phys.* **1998**, *108*, 4439. (c) Stratman, R. E.; Scuseria, G. E.; Frisch, M. J. *J. Chem. Phys.* **1998**, *109*, 8218.
(19) Mulliken, R. S. *J. Chem. Phys.* **1955**, *23*, 1833.
(20) orbpopg03, Jeffrey Hay, University of California, 2001.
(21) Otwinowski, Z.; Minor, W. *Methods in Enzymology, Vol 276: Macromolecular Crystallography, part A, 307−326, 1997*; Carter, Jr., C. W., Sweet, R. M., Eds.; Academic Press: New York, 1997.
(22) Sheldrick, G. M. Institüt für Anorganische Chemie der Universität, Göttingen, 1998.
(23) Farrugia, L. J. *J. Appl. Crystallogr.* **1999**, *32*, 837.

Table 2. Observed Spectroscopic and Geometric Parameters for $MM'(O_2C^tBu)_4$ Complexes (M, M′ = Mo, W) and Their Single-Electron Oxidation Products; Calculated Values for the Model Complexes $MM'(O_2CCH_3)_4$ (M, M′ = Mo, W) Are Given in Parentheses

compound	d(MM)/Å	d(M−O)/Å[a,b]	ν(MM)/cm^{-1}	$\lambda_{max}(\delta\rightarrow\delta^*)$/nm
$Mo_2(O_2C^tBu)_4$[c]	2.087 (2.114)	2.11 (2.12)	403 (464)	430 (513)
$MoW(O_2C^tBu)_4$	2.0877(3) (2.158)	2.09 (2.13) (M = Mo) 2.09 (2.10) (M = W)	371 (419)	440 (489)
$W_2(O_2C^tBu)_4$	2.1767(3) (2.196)	2.08 (2.11)	318 (324, 366)	obscured (467)
$Mo_2(O_2C^tBu)_4^+PF_6^-$[d]	2.1512(5) (2.158)	2.08 (2.09)	387 (447)	760 (928)
$MoW(O_2C^tBu)_4^+PF_6^-$	unknown (2.197)	unknown (2.11, M = Mo) (2.06, M = W)	obscured (332, 402)	678 (697)
$W_2(O_2C^tBu)_4^+PF_6^-$	2.2094(3) (2.224)	2.06 (2.09)	obscured (332)	760 (709)

[a] Average values of all M−O distances. [b] While each calculated M−O(CO_2) bond is different by symmetry, only one M−O bond length is shown. The two values differed, at most, by 0.003 Å. [c] Average bond lengths obtained from three different polymorphs in refs 28 and 29. [d] Bond lengths from ref 9.

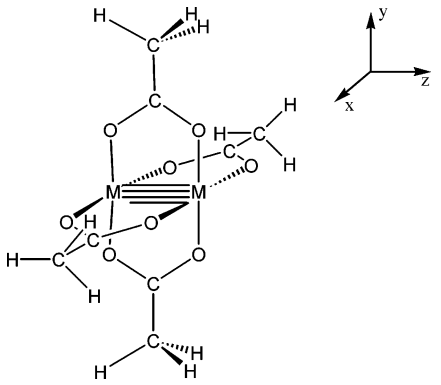

Figure 1. $M_2(O_2CMe)_4$ in C_{4v} symmetry.

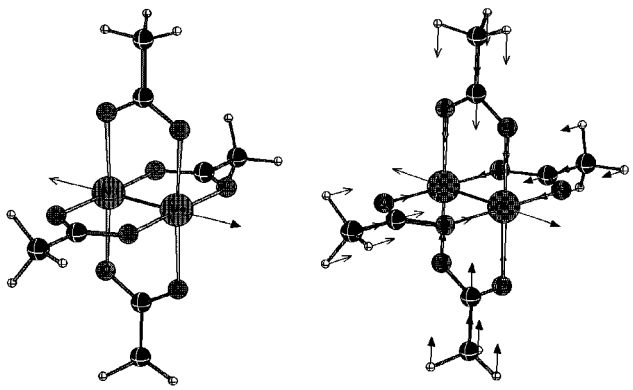

Figure 2. (a) Calculated symmetric ν(Mo−Mo) with displacement vectors. (b) Calculated lower energy symmetric ν(W−W) showing strong, antisymmetric coupling to ν(M−O).

orbital. There is also a small reduction in M−O distance due to the increase in effective charge on the metal and the fact that the δ bonding electrons are antibonding with respect to the metal−oxygen p_π orbitals.

A Mulliken population analysis[19] on the $MoW(O_2CMe)_4$ molecule and its radical cation showed a larger contribution of Mo orbital character to the M_2 δ HOMO relative to W. Specifically, for $MoW(O_2CMe)_4^+$ the δ orbital is found to be 46% Mo(d_{xy}) in character and 30% W(d_{xy}) in character, with the remaining orbital contributions centered on the acetate ligands. Similar orbital contributions are seen for $MoW(O_2CMe)_4$ [45% Mo(d_{xy}) and 32% W(d_{xy})].

The values of ν(MM) listed in Table 2 represent those modes that are identified as being principally localized on the two metals and being most Raman active. The Mo_2 stretching vibration in $Mo_2(O_2CMe)_4$ is shown in vector form in Figure 2 and is clearly seen to be Mo_2 localized. However, for $W_2(O_2CMe)_4$ and the $MoW(O_2CMe)_4^+$ cation, the MM stretching mode is strongly coupled to ν(M−O) stretches such that both modes are strongly Raman active.[24] These are also shown in vector form in Figure 2. In the higher energy mode, ν(MM) and ν(M−O) are coupled in a symmetric manner, while for the lower energy mode, the ν(MM) and ν(M−O) vibrations are of opposite phase.

It is instructive to note that the computational results presented in Table 2 reflect the experimental trends—observed on going from a neutral species to its radical cation—in the broadest sense. It can be readily seen that bond lengths decrease; the energies of ν(MM) decrease (notice they are coupled to M−O stretches in two cases); and the energies of the $\delta\rightarrow\delta^*$ transitions red shift, all upon oxidation by one electron. While the trends are readily apparent, it is also obvious the calculated values differ from the experimental ones, sometimes substantially. There is a caveat, however, in directly comparing the raw energies of calculated spectroscopic observables to experimental results. The model systems herein are treated in the gas phase using only one level of theory, albeit one documented to give good results for related metal−metal quadruply bonded systems.[17,25] There are also comparatively few studies which rigorously treat open-shell transition metal systems using TD-DFT, and this is an area of active research.[26] To address such issues, a much more comprehensive treatment of the effects of choice of density functional and basis set are currently under way.[27]

Solid-State Structures and Raman Spectral Data. To provide an experimental comparison to the calculated geometries of the acetate model compounds, single-crystal X-ray diffraction studies were performed on $MoW(O_2C^tBu)_4$, $W_2(O_2C^tBu)_4$, and $W_2(O_2C^tBu)_4^+PF_6^-$.

(24) Clark, R. J. H.; Hempleman, A. J.; Kurmoo, M. *J. Chem. Soc., Dalton Trans.* **1988**, 973.

(25) (a) Bursten, B. E.; Chisholm, M. H.; Clark, R. J. H.; Firth, S.; Hadad, C. M.; MacIntosh, A. M.; Wilson, P. J.; Woodward, P. M.; Zaleski, J. M. *J. Am. Chem. Soc.* **2002**, *124*, 3050. (b) Bursten, B. E.; Chisholm, M. H.; Clark, R. J. H.; Firth, S.; Hadad, C. M.; Wilson, P. J.; Woodward, P. M.; Zaleski, J. M. *J. Am. Chem. Soc.* **2002**, *124*, 12244. (c) Cotton, F. A. *J. Am. Chem. Soc.* **2003**, *125*, 8900. (d) Cotton, F. A.; Liu, C. Y.; Murillo, C. A.; Villagran, D.; Wang, X. *J. Am. Chem. Soc.* **2003**, *125*, 13564.

(26) Rinkevicius, Z.; Tunell, I.; Salek, P.; Vahtras, O.; Agren, H. *J. Chem. Phys.* **2003**, *119*, 34.

(27) Chisholm, M. H.; D'Acchioli, J. S. Unpublished results.

The molecular structure of $MoW(O_2C^tBu)_4$ has been previously reported.[30] The molecule contained a crystallographically imposed center of inversion, and hence the Mo and W atoms were modeled as being equally disordered on the same atomic site. This yielded a Mo−W bond length of 2.080(1) Å, which is unexpectedly shorter than that seen in the three polymorphs found for $Mo_2(O_2C^tBu)_4$ [2.087 Å (average)].[28,29] A new study was performed on $MoW(O_2C^tBu)_4$ in order to try to resolve the disorder of the metal atoms and thereby obtain a more representative Mo−W bond length. Crystals of $MoW(O_2C^tBu)_4$ were grown by layering a toluene solution of the compound with hexanes. The molecule once again contains a crystallographically imposed center of inversion, and unfortunately each Mo and W atom was disordered over the same atomic site, giving a similar Mo−W bond length [2.0877(3) Å] to that of the previous polymorph. All other bond lengths and angles within the molecule are unremarkable and can be obtained from the Supporting Information. The molecules pack in an analogous manner to that seen previously for $M_2(O_2CR)_4$ compounds, by way of intermolecular M···O interactions.[28,29]

Crystals of $W_2(O_2C^tBu)_4$ were also grown by layering a toluene solution of the compound with hexanes. The crystal lattice again shows chains of molecules formed by intermolecular W···O interactions, and relevant bond lengths and angles for this molecule can be obtained from the Supporting Information. The W−W bond length of 2.1767(3) Å is shorter than that reported for the related phosphine adduct $W_2(O_2C^tBu)_4 \cdot 2PPh_3$ [2.218(1) Å].[12]

Crystals of $W_2(O_2C^tBu)_4^+PF_6^-$ were obtained by oxidizing a suspension of $W_2(O_2C^tBu)_4$ in dichloromethane with 1 equiv of $FeCp_2PF_6$ and layering the resulting green solution with hexanes. As noted in the preparation of $Mo_2(O_2C^tBu)_4^+PF_6^-$,[9] significant quantities of a brown precipitate were also formed alongside green crystals of $W_2(O_2C^tBu)_4^+PF_6^-$, and no attempts were made to cleanly isolate the product. The structure revealed a W−W bond length of 2.2094(3) Å, roughly 0.03 Å longer than that of the neutral analogue. This is consistent with the decrease in bond order from 4 to 3.5 upon the removal of one electron from the tungsten δ orbital, although the increase is less than that observed upon oxidation of $Mo_2(O_2C^tBu)_4$ (0.06 Å). The WW distance is also still shorter than that in the neutral triphenyl phosphine adduct, which emphasizes the inherent problems that can be encountered if MM distance alone is used as a criteria for determination of MM electronic configuration in linked M_2 quadruply bonded compounds and their radical cations. Inspection of the packing diagram reveals that each W_2 unit is nestled between two PF_6^- anions which, by way of W···F interactions [W1···F1 = 2.689(3) Å], propagate an alternating $W_2(O_2C^tBu)_4^+\cdots PF_6^-$ chain in the solid state, as displayed in Figure 3. Despite numerous attempts, crystals of $MoW(O_2C^tBu)_4^+PF_6^-$ suitable for X-ray diffraction could not be isolated.

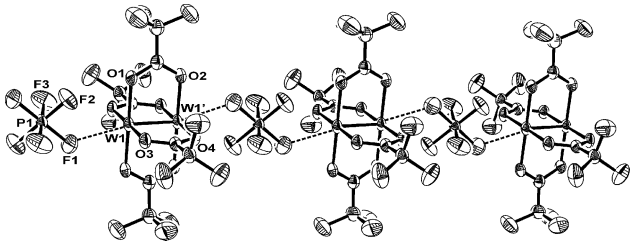

Figure 3. Crystal packing diagram for $W_2(O_2C^tBu)_4^+PF_6^-$ showing an alternating cation−anion chain by way of tungsten−fluorine interactions.

The experimental data for the geometric parameters and ν(MM) stretching modes of $M_2(O_2C^tBu)_4$ (M = Mo, W), $MoW(O_2C^tBu)_4$, and their related radical cations are presented in Table 2. It can be seen that as the MM distance increases, there is a concomitant decrease in the ν(MM) stretching energy. The ν(MM) stretching modes were not observed for the radical cations of $MoW(O_2C^tBu)_4$ and $W_2(O_2C^tBu)_4$, as they were obscured by the laser line filter below 300 cm^{-1}. The trends observed experimentally between bond lengths and MM stretching frequencies correlate well with those seen for the calculated data of the model acetate compounds in the gas phase, shown in Table 2.

The $\delta \rightarrow \delta^*$ Transition. The singlet $\delta \rightarrow \delta^*$ transition for $Mo_2(O_2C^tBu)_4$ and $MoW(O_2C^tBu)_4$ appear at 440 nm as a weak absorption ($\epsilon \sim 100$ M^{-1} cm^{-1}) due to the poor overlap of the δ-bonding orbitals. For $W_2(O_2C^tBu)_4$, this electronic transition is not observed because it is obscured by the much more intense W_2 $\delta \rightarrow CO_2$ π^* MLCT transition that has an absorption maximum at 360 nm, but tails to longer wavelength.

In the oxidized cations the $^2(\delta \rightarrow \delta^*)$ transition occurs at lower energy relative to the $^1(\delta \rightarrow \delta^*)$ transition for reasons that have been well-discussed in the literature.[31] Indeed, the $^2(\delta \rightarrow \delta^*)$ transition energy provides a more realistic value for the importance of the δ bond since the $^1(\delta \rightarrow \delta^*)$ transition energy is dominated by two electron contributions. The homonuclear cations $M_2(O_2C^tBu)_4^+$ where M = Mo or W, both show this absorption at around 760 nm, but the heteronuclear cation $MoW(O_2C^tBu)_4^+$ has this absorption at somewhat higher energy, at 678 nm (see Figure 4). We expect a significant dipole change with this excitation as in the ground state, the δ bond is polarized $Mo^{\delta-}$ and $W^{\delta+}$ whereas in the photoexcited state, it will be $W^{\delta-}$ and $Mo^{\delta+}$. It is quite possible that the polarity of this bond is creating the larger photoexcitation energy in the heteronuclear cation.

Electrochemistry and Electron Paramagnetic Resonance Spectroscopy. While the electrochemical properties of the homometallic complexes $M_2(O_2CR)_4$ (M = Mo, W) have been extensively investigated,[12,32] it is surprising to find no studies of the electrochemistry of the heteronuclear analogues $MoW(O_2CR)_4$. A cyclic voltammogram (CV) of

(28) Cotton, F. A.; Extine, M.; Gage, L. D. *Inorg. Chem.* **1978**, *17*, 172.
(29) Martin, D. S.; Huang, H.-W. *Inorg. Chem.* **1990**, *29*, 3674.
(30) Katovic, V.; McCarley, R. E. *J. Am. Chem. Soc.* **1978**, *100*, 5586.
(31) (a) Solomon, E. I.; Lever, A. B. P. *Inorganic Electronic Structure and Spectroscopy*; John Wiley and Sons: New York, 1999; Vol. 2. (b) Hopkins, M. D.; Gray, H. B.; Miskowski, V. M. *Polyhedron* **1987**, *6*, 705.
(32) (a) Zietlow, T. C.; Klendworth, D. D.; Nimry, T.; Salmon, D. J.; Walton, R. A. *Inorg. Chem.* **1981**, *20*, 947. (b) Cotton, F. A.; Pederson, E. *Inorg. Chem.* **1975**, *14*, 399. (c) Cayton, R. H.; Chisholm, M. H.; Huffman, J. C.; Lobkovsky, E. B. *J. Am. Chem. Soc.* **1991**, *113*, 8709.

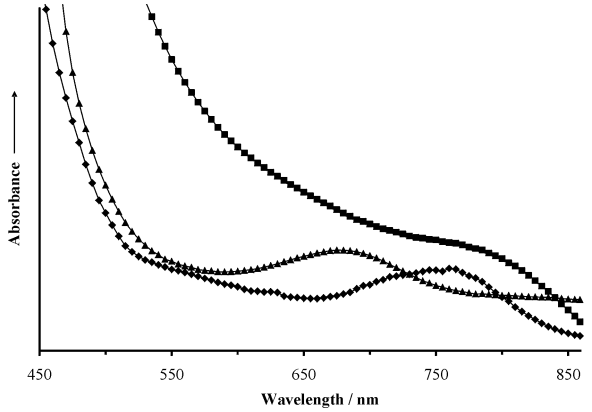

Figure 4. UV/Vis spectra of $Mo_2(O_2C^tBu)_4^+PF_6^-$ (◆), $MoW(O_2C^tBu)_4^+PF_6^-$ (▲), and $W_2(O_2C^tBu)_4^+PF_6^-$ (■) in dichloromethane.

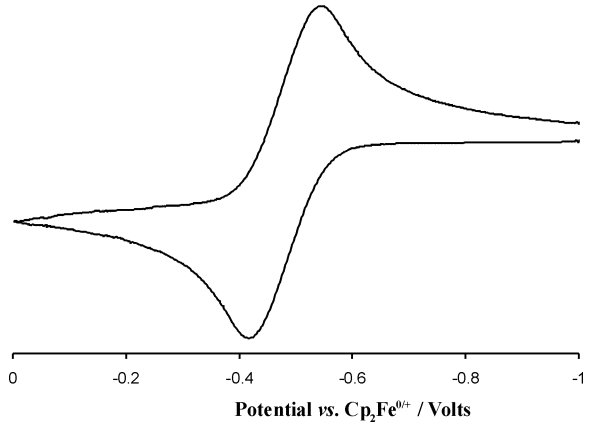

Figure 5. Cyclic voltammogram of $MoW(O_2C^tBu)_4$. Scan rate is 100 mV s^{-1}, and the electrolyte solution is 0.1 M $N^nBu_4PF_6$ in THF.

$MoW(O_2C^tBu)_4$ in a 0.1 M $N^nBu_4PF_6$ THF solution, acquired at a scan rate of 100 mV s^{-1}, is depicted in Figure 5. CV and differential pulse voltammetry (DPV) indicate the presence of one reversible oxidation process within the electrolyte window, at a potential of −0.48 V (vs $Cp_2Fe^{0/+}$).

The potential for $MoW^{4+/5+}$ lies between that of $Mo_2^{4+/5+}$ (−0.04 V) and $W_2^{4+/5+}$ (−0.70 V) but is closer to the tungsten potential. From this one might wish to infer that tungsten carries the greater positive charge in the radical cation and the electron density in the singly occupied δ orbital is polarized toward molybdenum. EPR spectroscopy clarifies this point (vide infra).

Chemical oxidation of the $MM'(O_2C^tBu)_4$ (M, M′ = Mo or W) complexes with Cp_2FePF_6 in CH_2Cl_2 yields the radical cations $MM'(O_2C^tBu)_4^+$, with PF_6^- counterions. These radical cations are unstable; hence, the oxidized species were generated in situ prior to any physical measurements. The species were investigated by EPR spectroscopy, and the solution spectra of the homometallic cations in 2-MeTHF are presented in Figure 6, and the results are summarized in Tables 3 and 4. The signal of the molybdenum species has $g_{iso} = 1.941$ and $A_{iso} = 27.0$ G for the ^{95,97}Mo isotopes, $I = {}^5/_2$, of 25.4% combined natural abundance. The signal of the tungsten species has $g_{iso} = 1.814$ and hyperfine lines with A = 51.0 G from the ^{183}W isotope, of 14.3% natural abundance with $I = {}^1/_2$. These A and g values, and the intensity of the hyperfine lines, agree with expectations for an unpaired electron completely delocalized over two molybdenum or two tungsten atoms. Components of g and A perpendicular and parallel to the MM axis have been resolved from the frozen solution spectrum of $W_2(O_2C^tBu)_4^+PF_6^-$.

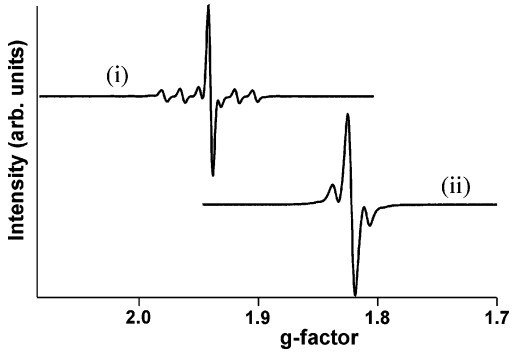

Figure 6. Solution EPR spectra of $Mo_2(O_2C^tBu)_4^+PF_6^-$ (i) and $W_2(O_2C^tBu)_4^+PF_6^-$ (ii) in CH_2Cl_2 at 210 K.

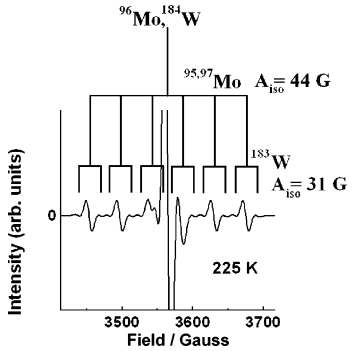

Figure 7. EPR spectrum of $MoW(O_2C^tBu)_4^+PF_6^-$ in 2-MeTHF solution at 225 K.

Table 3. Solution EPR Parameters of $MM'(O_2C^tBu)_4^+$ (M/M′ = Mo, W) Radical Cations in 2-MeTHF at 210 K

compound	g_{iso}	$A_{iso,Mo}$/G	$A_{iso,W}$/G
$Mo_2(O_2C^tBu)_4$	1.941	27.0	
$MoW(O_2C^tBu)_4$	1.881	44.1	31.0
$W_2(O_2C^tBu)_4$	1.814		51.0

Table 4. EPR Parameters of $MoW(O_2C^tBu)_4^+PF_6^-$ and $W_2(O_2C^tBu)_4^+PF_6^-$ in 2-MeTHF Glasses at 120 K

parameter	$MoW(O_2C^tBu)_4^+PF_6^-$	$W_2(O_2C^tBu)_4^+PF_6^-$
g_{iso}	1.883	1.817
$g_{\|\|}$	1.895	1.8216
$g_\perp$	1.878	1.8145
$A_{iso,Mo}$/G	47.6	
$A_{\|\|,Mo}$/G	58.8	
$A_{\perp,Mo}$/G	41.4	
$A_{iso,W}$/G	31.6	51.1
$A_{\|\|,W}$/G		66.7
$A_{\perp,W}$/G		43.3

The fluid solution EPR spectrum of $MoW(O_2C^tBu)_4^+PF_6^-$, depicted in Figure 7, contains a six-line pattern of hyperfine lines, in addition to the central line, originating from coupling of the electron to the spin-active isotopes ^{95,97}Mo. Further splitting is evident from molecules containing a spin-active ^{183}W. The A values associated with these splittings are $A_{iso,Mo}$ = 44 G and $A_{iso,W}$ = 31 G. The fact that the magnitude of

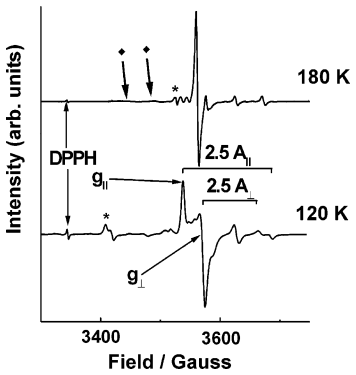

Figure 8. X band (9.5 GHz) spectrum of $MoW(O_2C^tBu)_4^+PF_6^-$ at 180 K (solution) and 120 K (frozen glass). The spectrum at 180 K clearly shows the broadening of the low-field hyperfine peaks (indicated by ◆) corresponding to the $^{95(97)}$Mo nucleus. The 120 K spectrum depicts the anisotropy in both g ($g_{||} = 1.8945$ and $g_\perp = 1.878$) and A_{Mo} ($A_{||} = 59$ G and $A_\perp = 41$ G) and establishes the sign of $\beta = (g_{||} - g_\perp)(A_{||} - A_\perp)$ as positive (see text). Peaks due to impurities are marked by asterisks.

$A_{iso,Mo}$ is greater than that of $Mo_2(O_2C^tBu)_4^+$, and the fact that the magnitude of $A_{iso,W}$ is less than that of $W_2(O_2CBu^t)_4^+$, indicates that the unpaired electron of $MoW(O_2C^tBu)_4^+$ resides in an orbital with greater Mo $4d_{xy}$ relative W $5d_{xy}$ character. Specifically, modeling indicates 71% Mo and 29% W atomic orbital contribution.

The frozen solution EPR spectrum of $MoW(O_2C^tBu)_4^+PF_6^-$, like that of $W_2(O_2C^tBu)_4^+PF_6^-$, may be fit with axially symmetric A and g tensors, with the principal elements listed in Table 4. Our resolution was insufficient to determine the values of $A_{||}$ and $A_\perp$ for ^{183}W in the MoW^{5+} complex.

Figure 8 shows the X-band (9.5 GHz) EPR spectra of $MoW(O_2C^tBu)_4^+PF_6^-$ taken at 180 K (solution) and 120 K (frozen glass). Evidenced in the 180 K spectrum, the low-field hyperfine transitions broaden with lowering temperature. The width of the hyperfine peaks can be related to the anisotropy in g and A, as shown below:

$$\Gamma = \alpha + \beta M_I + \gamma M_I^2 \quad (1)$$

where Γ is the width of a given hyperfine transition, β is a measure of both g and hyperfine anisotropies [$\beta \propto (g_{||} - g_\perp)(A_{||} - A_\perp)$], α is the line-broadening effects that remain constant for all values of M_I, γ is a function of the hyperfine anisotropy, and M_I is the nuclear spin quantum number.[33,34] Therefore, the determination of the anisotropic components of both g and A allows for the designation of the hyperfine peaks to specific M_I values.

The EPR spectrum of $MoW(O_2C^tBu)_4^+PF_6^-$ acquired at 120 K (frozen glass) clearly shows the anisotropy in both g ($g_{||} = 1.895$ and $g_\perp = 1.878$) and A_{Mo} ($A_{||} = 58.8$ G and $A_\perp = 41.4$ G) and yields the sign of β as positive. Following (1), the larger peak widths of the low-field hyperfine transitions allow them to be assigned to the positive M_I values of the ^{95,97}Mo nuclei. Specific assignment of the hyperfine transitions allows us to determine the sign of the isotropic hyperfine coupling constant A_{iso}, as given by the isotropic spin Hamiltonian of an $S = {}^1/_2$ system:

$$\mathscr{H} = g\mu_B H \cdot S + A_{iso} \cdot S \cdot I \quad (2a)$$

$$E = g\mu_B H M_s + A_{iso} M_s M_I \quad (2b)$$

In the above expression, the first term is the Zeeman energy while the second term is the isotropic hyperfine coupling interaction. According to (2), the position of the positive M_I hyperfine transitions indicates that the absolute sign of A_{iso} is positive. The absolute sign of A_{iso} can then be related to the electron density present on the ^{95,97}Mo nuclei, $\psi(0)$, as given by[34]

$$A_{iso} = (2/3)\mu_0 g \mu_B g_n \mu_n |\psi(0)|^2 \quad (3)$$

Here, μ_0 is the permittivity of free space (12.566×10^{-7} J C^{-2} s^2 m^{-1}), μ_B is the Bohr magneton (9.274×10^{-24} J T^{-1}), g_n is the nuclear g factor of the ^{95,97}Mo nuclei (-0.3656, -0.3734), and μ_n is the nuclear magneton (5.0508×10^{-27} J T^{-1}). Therefore, the negative value of g_n for the two Mo isotopes, along with the positive value of A_{iso}, indicates that the hyperfine coupling about the Mo nucleus originates from the polarization of the inner s electrons by the outer 4d electrons.

Concluding Remarks

The data reported here should assist in the characterization of mixed valence compounds of molybdenum or tungsten of the type $[(^tBuCO_2)_3M_2]_2(\mu\text{-}O_2C{-}X{-}CO_2)^+$ as Class II or III. Also of particular interest are the spectroscopic data for the $MoW(O_2C^tBu)_4^+$ cation that reveals evidence of the polarity of the δ orbital from EPR and electronic absorption spectroscopy.

Acknowledgment. We thank the National Science Foundation for support and gratefully acknowledge the Ohio Supercomputer Center for computational resources. Dr. Judith Gallucci is thanked for her assistance in obtaining the crystallographic data. Professors Jeffrey Zaleski and Richard McCreery are thanked for assistance on obtaining the Raman spectra and Professor Christopher Hadad for guidance with computational procedures. N.D. would like to thank the National Science Foundation (NIRT Grant No. DMR 0103290) for financial support.

Supporting Information Available: CIF file containing the three crystal structures reported in this paper, as well as structure drawings (Figures S1−S3) and tables of selected bond lengths and angles (Tables S1−S3).

IC049081G

(33) Dalal, N. S.; Millar, J. M.; Jagadeesh, M. S.; Seehra, M. S. *J. Chem. Phys.* **1981**, *74*, 1916.
(34) Weil, J. A.; Bolton, J. R.; Wertz, J. E. *Electron Paramagnetic Resonance*; John Wiley and Sons: New York, 1994.